OPEN ACCESS

CORRELATION OF YOUNG'S MODULUS WITH BONE MINERAL DENSITY IN ANIMAL BONES VIA QCT

Leszek Pyziak[1][https://orcid.org/0000-0003-4898-8911], *Tomasz Więcek*[1][https://orcid.org/0000-0002-4776-9357], *Sławomir Wolski*[2][https://orcid.org/0000-0002-8968-0959], *Piotr Biega*[2][https://orcid.org/0000-0002-3484-6042], *Michał Wanic*[2][https://orcid.org/0000-0002-4905-4988]

[1]*Department of Applied Optics, The Faculty of Mathematics and Applied Physics, Rzeszow University of Technology, Poland*

[2]*Department of Physics and Medical Engineering, The Faculty of Mathematics and Applied Physics, Rzeszow University of Technology, Poland.*

Email: l.pyziak@prz.edu.pl

Abstract - In the present study, the methodology and results for determining the Young's modulus, a key physical parameter, and the bone mineral density (BMD) of the same specimens are presented. Young's modulus was measured using mechanical testing, and BMD was determined by quantitative computed tomography (QCT). The specimens were prepared from the cortical region of porcine femoral bones, sourced from animals which were approximately 1 and 3 years old at the time of slaughter. QCT measurements were performed using two distinct X-ray tube settings of the computed tomography scanner. The investigation aimed to identify correlations between BMD values obtained from QCT and the measured Young's modulus values. Additionally, the BMD results were compared for different scanner settings of the computed tomography system.

Keywords: Bone mineral density (BMD), Mechanical properties, Young's modulus, Quantitative computed tomography (QCT).

1. Introduction

One of the continuing challenges in medical diagnostics is the non-invasive or minimally invasive evaluation of bone fracture risk in pathological regions through the analysis of images derived by computed tomography. Efforts to establish correlations between the mechanical properties of bone tissue and diagnostic imaging have been described in the literature [1-6]. Quantitative computed tomography (QCT) serves as a primary method for predictive analyses. Many studies also present findings obtained from the finite element analysis (FEA) [1, 7, 8].

Pathological fractures most commonly occur in the regions of the hip joint and the spine [9]. In the context of osteoporosis, they represent a significant public health challenge associated with population aging and the increasing cost of treatment in this group of patients. Osteoporosis is a metabolic bone disease characterized by both qualitative and quantitative degradation of bone tissue. Primary osteoporosis is age-related, in contrast to secondary osteoporosis, which develops as a consequence of primary bone tumors, metastatic solid tumors, or their treatment. Pathological fractures lead to a deterioration in quality of life, increased dependency, reduced mobility, and complications, which generate substantial costs for healthcare systems [10]. The assessment of bone tissue strength to identify patients who require early intervention is essential for mitigating these adverse outcomes.

The strength of bone tissue depends on its microarchitecture, remodeling rate, cumulative microdamage, and bone mineral content [11]. Bone mineral density (BMD) is a widely recognized parameter used to assess bone strength [3]. Several radiographic techniques have been developed to evaluate BMD, including dual-energy X-ray absorptiometry (DXA) [12] and quantitative computed tomography (QCT) [13]. However, BMD has been proven to have low specificity and sensitivity as a predictor when assessing fracture risk. This limitation is attributed to the complex structure of bone tissue, which must be taken into account in fracture risk assessment. According to the literature, while BMD correlates well with mechanical properties of bone (ex situ, r=0.9), it

https://doi.org/10.17683/ijomam/issue22.v1.12

predicts fracture risk in only 10–44% of patients [2]. In the remaining cases, fractures occur despite normal BMD values.

The implementation of the influence of bone tissue architecture in fracture risk is feasible through the application of finite element analysis (FEA) [14]. To this end, data obtained from computed tomography can be used to construct a mechanical model of the imaged vertebra and perform numerical simulations. However, the generated three-dimensional models of the analysed vertebrae require the inclusion of mechanical properties and boundary conditions to simulate in vivo fracture conditions with the highest possible precision [1, 4, 7, 15]. FEA-based models demonstrate superior performance in estimating fracture risk compared to models derived solely from computed tomography or those relying exclusively on BMD values.

Unfortunately, all these techniques rely on X-ray radiation, exposing patients to doses up to 360 μSv. Patient exposure to radiation is an unavoidable aspect that should be minimized. To reduce absorbed doses, low-dose computed tomography protocols have recently been introduced. Studies have also investigated the impact of exposure parameters on the assessment of BMD, fracture risk, mechanical properties, volumetric bone tissue characteristics, and imaging quality.

The aim of our study was to measure the Young's modulus of bone and to analyse its correlation with BMD values obtained from QCT images, performed using both low-dose and high-dose protocols. The data acquired during this study may contribute to the development of more accurate fracture risk models based on QCT scans.

2. Static Bending Test

Young's modulus (E), also referred to as the modulus of elasticity, is a fundamental mechanical property of materials that characterizes their elastic behaviour within the linear-elastic deformation range. It represents the ratio of stress (σ) to strain (ϵ) in the elastic region, as defined by Hooke's Law: E=σ/ϵ [16, 17]. One of the most commonly employed methods for determining Young's modulus in biological materials, such as bone, is the static three-point bending test [17]. In this method, a specimen supported at both ends is subjected to a force (P) applied at the midpoint of its length (Fig. 1).

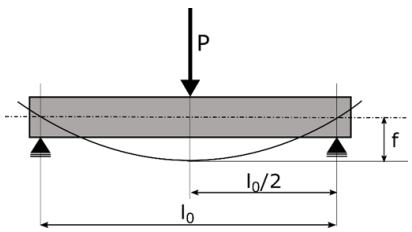

Figure 1: Diagram illustrating the three-point bending method

As a result of the applied force, the specimen undergoes deflection, measured as the deflection arrow (f), which can be described by a relationship derived from the theory of beam bending [18]:

$$f = \frac{P l_0^3}{48EI} \tag{1}$$

where:
P – applied load force (N),
l_0 – support span (mm),
E – Young's modulus (MPa lub GPa),
I – moment of inertia of the specimen's cross-sectional area (mm^4).

For a specimen with a rectangular cross-section, the moment of inertia is given by $I = \frac{bh^3}{12}$, where b is the width of the specimen, and h is its thickness. By applying this to equation (1), we obtain:

$$f = \frac{l_0^3}{4Ebh^3} \cdot P \tag{2}$$

Equation (2) is valid for small loads, i.e., within the so-called elastic range, and represents a linear relationship. By determining the value of the slope of the line (a) and comparing it with the fraction on the right-hand side of equation (2), the value of Young's modulus can be calculated:

$$E = \frac{l_0^3}{4bh^3} \cdot a \tag{3}$$

3. Quantitative Computed Tomography

Computed tomography (CT) is an advanced diagnostic technique that exploits the attenuation of an X-ray beam resulting from its absorption or scattering as it passes through the examined object. The degree of attenuation depends on the density and chemical composition of the tissue, including bone thickness and the content of mineral constituents such as hydroxyapatite [19].

This method enables the reconstruction of three-dimensional images of the investigated object by integrating projection images acquired from multiple angles, allowing for detailed analysis of anatomical structures with high spatial resolution [20]. Modern CT systems, equipped with advanced reconstruction algorithms, provide accurate visualization of both cortical and trabecular bone, which is of key importance in biomechanical and clinical studies [21].

Quantitative computed tomography (QCT) represents a specialized variant of CT, distinguished by the use of a calibration phantom scanned in parallel with the skeletal region under investigation. The calibration phantom, typically containing

reference materials of known densities (e.g., calcium phosphate at different concentrations), allows for the conversion of Hounsfield units (HU) into bone mineral density (BMD), expressed in mg/cm^3 (for volumetric analysis) or mg/cm^2 (for surface-based analysis) [13,22-24]. Based on the phantom reference densities, a calibration curve is generated, enabling precise determination of BMD in any region of the bone with a resolution corresponding to an individual voxel [25].

The accuracy of QCT measurements is particularly crucial in the diagnosis of osteoporosis, where reduced BMD correlates with an increased risk of fractures.

4. Preparation of Bone Specimens for Testing

Bone specimens were obtained from the cortical layer of femora obtained from pigs aged 1 and 3 years. In the first stage of preparation, the proximal and distal epiphyses were removed, leaving the femoral shafts for further processing. Each shaft was then longitudinally divided into four sections, followed by the removal of the bone marrow and residual soft tissues. The cleaned cortical fragments were subsequently shaped into rectangular parallelepipeds using a computer numerical control (CNC) milling machine. The specimen dimensions were maximized within the limits imposed by cortical thickness and the natural shape of the bone, resulting in some variation in the geometrical parameters among individual specimens.

After shaping, the specimens were stored in a frozen state at –20 °C, a procedure which, according to the literature, preserves the mechanical properties of bone for up to two years [26]. Freezing at this temperature minimizes alterations in the microstructure and biomechanical parameters, such as the Young's modulus, which is essential for ensuring reliable outcomes in both mechanical and densitometric analyses [27].

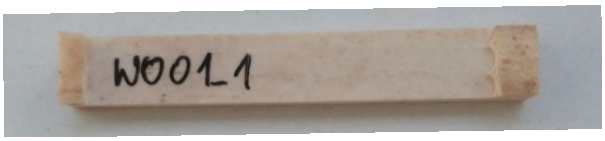

Figure 2: Appearance of a prepared bone specimen

The appearance of a representative bone specimen is shown in Figure 2, while the geometrical dimensions of the specimen cross-sections are summarized in Table 1. A total of 10 specimens were prepared, five of which were obtained from femora of 1-year-old pigs (labeled 1_1–1_5), and the remaining five from femora of 3-year-old pigs (labeled 3_1–3_5).

Table 1. Summary of samples and their geometric parameters

Material	Sample number	Thickness (h)	Width (b)
		mm	mm
Porcine bone from a 1-year-old animal	1_1	2.62	12.87
	1_2	2.01	12.48
	1_3	2.83	9.28
	1_4	3.31	9.27
	1_5	2.92	15.29
Porcine bone from a 3-year-old animal	3_1	1.94	11.40
	3_2	2.20	12.38
	3_3	3.17	9.63
	3_4	1.91	10.84
	3_5	1.96	8.74

5. Measurements

Bone mineral density (BMD) measurements of specimens prepared from the cortical layer of porcine femora were performed using quantitative computed tomography (QCT) on a Siemens SOMATOM Definition AS scanner. Two acquisition protocols were applied:

- Low-dose setting (BMD_L): tube voltage 100 kV, tube current-time product 24–29 mAs, typically used in medical diagnostics to minimize radiation dose.
- High-dose setting (BMD_H): tube voltage 120 kV, tube current-time product 160 mAs, providing images with higher spatial resolution and reduced noise.

The in-plane pixel was 0.44 × 0.44 mm^2 with a slice thickness of 0.6 mm. An Osteo reference phantom (Siemens Healthcare) was used for BMD calibration, consisting of two compartments: a water-equivalent insert corresponding to a density of 0 mg/cm^3, and a bone-equivalent section containing hydroxyapatite at 200 mg/cm^3 density. Based on the phantom data, a calibration curve was generated to convert Hounsfield units (HU) into BMD values (mg/cm^3) for selected regions of interest (ROI) of a comparable surface area. The conversion was performed using the manufacturer's software supplied with the CT scanner.

Representative QCT scans are shown in Figure 3, illustrating transverse views of the bone specimens (Figures 3a and 3c) with the reference phantom visible at the bottom of the section, and sagittal views of the same specimens (Figures 3b and 3d). Grayscale intensity in the images corresponds to BMD values, enabling visual assessment of the mineral density distribution within the specimens.

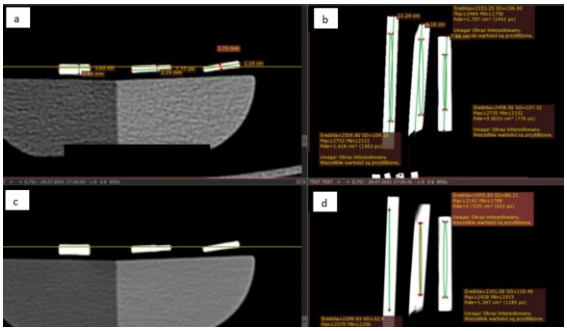

Figure 3: Representative computed tomography scans of bone tissue for exposures a, b) BMD_L and c, d) BMD_H, presented in a, c) axial view (with the phantom cross-section visible in the lower part) and b, d) sagittal view

The static three-point bending test was carried out using an INSTRON 5937 universal testing machine in accordance with the PN-EN 843-1:2007 standard. The following test parameters were applied:

- loading rate: 2 mm/min,
- support span: 50 mm,
- maximum bending force: 20 N,
- support diameter: 10 mm.

6. Discussion of the Results

For each bone specimen, two different bone mineral density (BMD) values were obtained depending on the QCT acquisition mode. In the low-dose measurement (BMD_L), the values were consistently higher compared with the high-dose setting (BMD_H). For both scanning modes, a weak positive linear relationship was observed between BMD and Young's modulus (E). The relationship between BMD and E for both exposure protocols is presented in Figure 4, and the measurement results are summarized in Table 2. Table 2 also includes the mean values of E, BMD_L, and BMD_H, along with their measurement uncertainties (shaded cells). It can be observed that, when taking into account the measurement uncertainties, the values of E, BMD_L, and BMD_H are consistent.

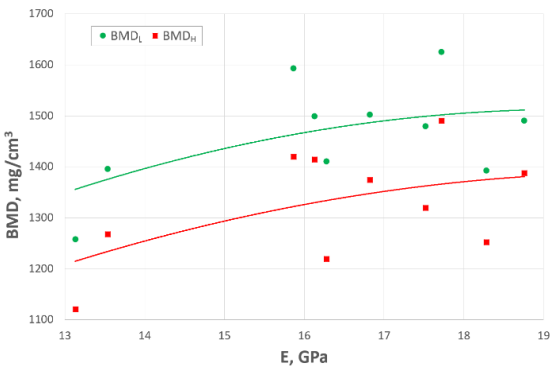

Figure 4: Bone Mineral Density as a function of Young's modulus for low-dose exposure and high-dose exposure

Table 2. Summary of specimens and obtained values of Young's modulus (E), BMD_L and BMD_H along with their mean values and uncertainties (shaded cells)

Material	Sample number	E	BMD_L	BMD_H
		GPa	mg/cm³	mg/cm³
Porcine bone from a 1-year-old animal	1_1	16.28	1410	1219
	1_2	17.52	1479	1319
	1_3	18.76	1490	1387
	1_4	13.13	1258	1121
	1_5	18.29	1392	1252
		16.8 ± 2.3	**1406 ± 93**	**1260 ± 101**
Porcine bone from a 3-year-old animal	3_1	15.87	1593	1420
	3_2	13.54	1395	1268
	3_3	17.72	1625	1490
	3_4	16.82	1502	1374
	3_5	16.13	1499	1414
		16.0 ± 1.6	**1523 ± 91**	**1393 ± 82**

The differences between the obtained values may result from variations in scanner settings, such as tube voltage (100 kV for BMD_L vs. 120 kV for BMD_H) and tube current (24–29 mAs for BMD_L vs. 160 mAs for BMD_H), which affect image contrast and noise [28]. The high-dose mode, due to its higher spatial resolution and lower noise, more accurately represents cortical layer density, whereas the low-dose mode, commonly used in medical diagnostics, may overestimate BMD due to noise and artifacts [21, 29]. An additional source of potential error in BMD measurements is the use of the Osteo reference phantom (Siemens Healthcare), which contains only two calibration fields with densities of 0 and 200 mg/cm^3. The cortical bone density of porcine femora, ranging from 1258–1625 mg/cm^3 for BMD_L and 1121–1490 mg/cm^3 for BMD_H (Table 2), substantially exceeds the phantom's calibration range. Linear interpolation between the 0 and 200 mg/cm^3 points may introduce approximation errors, particularly at high densities, thereby affecting the accuracy of BMD estimation. It is expected that a phantom with an extended density range (e.g., 0–2000 mg/cm^3) would enable precise BMD assessment in cortical bone. Phantom limitations may have contributed to the discrepancies between BMD_L and BMD_H and could have influenced the analysis of the relationship between BMD and the Young's modulus E.

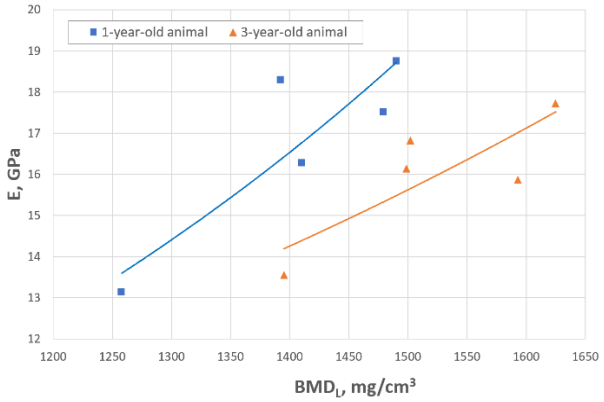

Figure 5: Relationship between Young's modulus (E) values and BMD$_L$ for porcine bones derived from a 1-year-old and 3-year-old animals.

For the analysis of the correlation between Young's modulus E and BMD$_L$, stratified by age groups, the results obtained using the low-dose setting commonly applied in diagnostic practice were used (Figure 5). The plots were generated for porcine bones from a 1-year-old animal (blue squares) and a 3-year-old animal (orange triangles), with fitted linear trend lines. A separation of BMD$_L$ values between age groups is evident, with higher values observed in 3-year-old animals, consistent with the literature indicating increased bone mineralization in older pigs due to a longer remodeling period [30]. Both E and BMD$_L$ values exhibit a relatively wide variability. In both age groups, E increases with increasing BMD$_L$. However, the absence of a clear dependence of E on animal age (the difference in means is only 0.8 GPa) suggests that cortical stiffness is more influenced by microstructural features (e.g., the spatial organization of osteons and collagen fibers) than by mineral content. These relationships are also illustrated in Figure 6, which presents the mean values of BMDL and Young's modulus (values taken from the grayed out cells of table 2) as a function of animal age. BMDL tends to increase with age [31], whereas Young's modulus exhibits a slight decline.

This correlation may reflect age-related alterations in the internal bone architecture, potentially resulting from increased mechanical loading. These findings are partially consistent with the study by Aerssens et al., who demonstrated that the mineral density of porcine bone increases with age, while changes in mechanical properties are less pronounced [32].

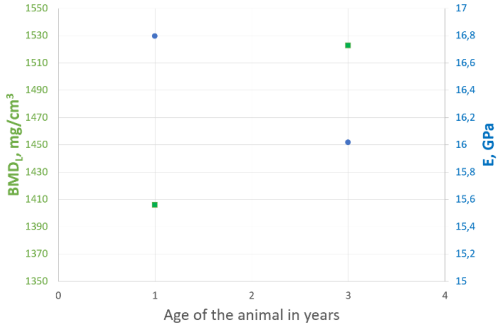

Figure 6: Dependence of the mean BMD$_L$ and mean Young's modulus E on animal age.

7. Summary

In this study, Young's modulus was measured using the three-point bending method on cortical samples from porcine femora obtained from 1- and 3-year-old animals, along with BMD measurements conducted using QCT. These values can be useful for numerical simulations aimed at predicting fracture risk.

Young's modulus was determined using a mechanical testing machine through three-point bending. Bone mineral density was measured under two different acquisition protocols: low-dose and high-dose. Identical BMD values were expected, as this parameter characterizes the intrinsic material properties of bone and should not depend on the scanner settings. Images acquired at higher energy exhibit reduced noise; however, due to the substantially increased radiation dose, such scanner settings are not employed in clinical practice. It was demonstrated that QCT measurements using higher-energy X-ray beams yielded BMD values different from those obtained with the low-dose protocol, regardless of the measured Young's modulus (Fig. 4). The BMD values were consistently lower at higher beam energy. This discrepancy may have been influenced by the QCT reference phantom, which contains only two calibration fields at 0 and 200 mg/cm^3, while the measured cortical bone density exceeded 1100 mg/cm^3.

Therefore, BMD values obtained with QCT at different X-ray energies should not be directly compared, and caution should also be exercised when comparing results from different CT scanners. Emphasis should be placed on the qualitative relationships between bone mineral density and other parameters.

Mechanical properties of bone, such as Young's modulus, are influenced by multiple factors, including age, nutrition, breed, rearing environment, and the internal bone structure. The porcine bones were obtained from different individuals, hence the observed variability in Young's modulus across samples is expected (Fig. 5).

Based on the initial results (Fig. 5), no clear correlation between Young's modulus and BMD can be observed. Determining BMD using QCT does not allow for unambiguous assignment of the corresponding Young's modulus values. BMD values clearly differ between 1- and 3-year-old animals, with higher Young's modulus observed in the 3-year-old group. This confirms the sensitivity of the QCT method in capturing age-related variations in BMD distribution, suggesting that similar differences could also be detected in pathologically altered human bones with heterogeneous microstructure.

Acknowledgements

This work is part of the research project N2_078 entitled: "Multiparametric Technology for Measurement and Assessment of Mechanical Properties."

References

[1] A. John, G. Kokot, „Identification of mechanical parameters of bone tissue as a base of numerical simulation in medicine," Archives of Materials Science and Engineering, tom 83, nr 2, pp. 49-67, 2017.

[2] H. Sievänen, „Bone densitometry and true BMD accuracy for predicting fractures: What are the alternatives?," Journal of Clinical Rheumatology, tom 5, pp. 371-385, 2010. doi: https://doi.org/10.2217/IJR.10.16

[3] K. N. Haseltine, T. Chukir, P. J. Smith, J. T. Jacob, J. P. Bilezikian, A. Farooki, „Bone Mineral Density: Clinical Relevance and Quantitative Assessment," J Nucl Med., tom 62, nr 4, Apr 2021. doi:https://doi.org/10.2967/jnumed.120.256180.

[4] M. Mirzaei, M. Keshavarzian, F. Alavi, „QCT-based failure analysis of proximal femurs under various loading orientations," Med Biol Eng Comput, tom 53, p. 477–486, 2015. doi: https://doi.org/10.1007/s11517-015-1254-2

[5] R. S. L. Resmi, V. Hashim, J. Mohammed, i P. N. Dileep, „A novel approach by integrating CT-based imaging data and machine learning to predict patient-specific Young's modulus values," Front. Bioeng. Biotechnol., vol. 13, 2025, Art. no. 1411291. https://doi.org/10.1155/aort/6257188

[6] B. Namiranian, K. Doi, S. Alenezi, S. B. Shah, S. Jerban, i E. Y. Chang, „Bone evaluation with micro finite element analysis in animal models," Tomography, vol. 11, no. 9, pp. 101, Sep. 2025. https://doi.org/10.3390/tomography11090101

[7] N. K. Knowles, J. M. Reeves, L. M. Ferreira, „Quantitative computed tomography (QCT) derived bone mineral density (BMD) in finite element studies: a review of the literature," J Orthop Surg Res, tom 3, nr 36, Dec 2016. doi: https://doi.org/10.1186/s40634-016-0072-2 .

[8] D. Subramaniam, F. Mat, M.S.A. Majid, et al. Finite element analysis of proximal femur in sideways fall under quasi-static loading. J Mech Sci Technol 37, 3315–3325 (2023). https://doi.org/10.1007/s12206-023-2210-y

[9] E. Mehnert, F. Möller, C. Hofbauer, e. al., „Palliative care of proximal femur metastatic disease and osteolytic lesions: results following surgical and radiation treatment," BMC Cancer, tom 24, nr 1431, 2024. doi: https://doi.org/10.1186/s12885-024-13170-0.

[10] R. Huo, C. Wei, X. Huang, Y. Yang, X. Huo, D. Meng, R. Huang, Y. a. Z. X. Huang, Y. Yang, „Mortality associated with osteoporosis and pathological fractures in the United States (1999–2020): a multiple-cause-of-death study," Journal of orthopaedic surgery and research, tom 19, nr 568, 2024. doi: https://doi.org/10.1186/s13018-024-05068-1.

[11] J.-Y. Rho, L. Kuhn-Spearing, P. Zioupos, „Mechanical properties and the hierarchical structure of bone," Medical Engineering & Physics, tom 20, p. 92–102, 1998. doi: https://doi.org/10.1016/S1350-4533(98)00007-1.

[12] R. L. Ramos, J. A. Armán, N. A. Galeano, A. M. Hernández, J. G. Gómez, J. G. Molinero, „Dual energy X-ray absorptimetry: fundamentals, methodology, and clinical applications," Radiologia, tom 54, nr 5, pp. 410-423, Sep-Oct 2012. doi: https://doi.org/10.1016/j.rxeng.2011.09.005.

[13] J. E. Adams, „Quantitative computed tomography," European Journal of Radiology, tom 71, nr 3, p. 415–424, Sep 2009. doi: https://doi.org/10.1016/j.ejrad.2009.04.074.

[14] L. D. Carbonare, S. Giannini, „Bone microarchitecture as an important determinant of bone strength," J Endocrinol Invest., tom 27, nr 1, pp. 99-105, Jan 2004. doi: https://doi.org/10.1007/BF03350919.

[15] M. B. Ogurkowska, A. Błaszczyk, „Distribution of Young's modulus at various sampling points in a human lumbar spine vertebral body," The Spine Journal, tom 20, nr 11, p. 1861–1875, 2020. doi: https://doi.org/10.1016/j.spinee.2020.06.013.

[16] F.P. Beer, E.R. Johnston Jr., J. T. DeWolf, i D. F. Mazurek, Mechanics of Materials, 8th ed. New York, NY, USA: McGraw-Hill Education, 2020.

[17] W.D. Callister Jr. i D.G. Rethwisch, Materials Science and Engineering: An Introduction, 10th ed., NJ, USA: Wiley, 2024.

[18] A. C. Ugural i S. K. Fenster, Advanced Mechanics of Materials and Applied Elasticity, 6th ed. Hoboken, NJ, USA: Pearson, 2023.

[19] J.T. Bushberg, J.A.Seibert, E.M. Leidholdt Jr., J.M. Boone, The Essential Physics of Medical Imaging (4th Edition), Lippincott Williams & Wilkins, 2021.

[20] W. Kalender, Computed tomography: fundamentals, system technology, image quality, applications. 3rd rev, Erlangen: Publicis Corporate Pub., 2011. doi: https://doi.org/10.1258/ar.2012.12a010.

[21] K. Engelke, T. Lang, S. Khosla, L. Qin, P. Zysset, W. D. Leslie, J. A. Shepherd, J. T. Schousboe, „Clinical Use of Quantitative Computed Tomography (QCT) of the Hip in the Management of Osteoporosis in Adults: the 2015 ISCD Official Positions—Part I," Journal of Clinical Densitometry, tom 18, nr 3, pp. 338-358, 2015. https://doi.org/10.1016/j.jocd.2015.06.012.

[22] C. E. Cann, H. K. Genant, „Precise measurement of vertebral mineral content using computed tomography," J Comput Assist Tomogr, tom 4, nr 4, pp. 493-500, 1980. doi: https://doi.org/10.1097/00004728-198008000-00018.

[23] P. B., Radiologia: diagnostyka obrazowa, Warszawa: PZWL, 2014.

[24] J.-Y. Rho, M. Hobatho, R. Ashman, „Relations of mechanical properties to density and CT number in human bone," Med Eng Phys, tom 17, nr 5, pp. 347-355, Jul 1995. doi: https://doi.org/10.1016/1350-4533(95)97314-f.

[25] L. McNamara, P. Prendergast, M. Schaffler, „Bone tissue material properties are altered during osteoporosis," Musculoskeletal Neuronal Interact, tom 5, nr 4, pp. 342-343, Oct-Dec 2005.

[26] C. Fölsch, W. Mittelmeier, U. Bilderbeek, N. Timmesfeld, T. von Garrel, H. P. Matter, „Effect of Storage Temperature on Allograft Bone," Transfus Med Hemother, tom 39, nr 1, p. 36–40, 2012. doi: https://doi.org/10.1159/000335647.

[27] E. H. van Haaren, B. C. van der Zwaard, A. J. van der Veen, I. C. Heyligers, P. I. Wuisman, T. H. Smit, „Effect of long-term preservation on the mechanical properties of cortical bone in goats," Acta Orthop., tom 79, nr 5, pp. 708-716, 2008. https://doi.org/10.1080/17453670810016759

[28] H. Giambini, D. Dragomir-Daescu, P. Huddleston, J. Camp, K. An, A. Nassr, „The effect of quantitative computed tomography acquisition protocols on bone mineral density estimation," J Biomech Eng, tom 137, nr 11, 2015. doi: https://doi.org/10.1115/1.4031572.

[29] C. Brunnquell, D. Ba, S. Khosla, e. al., „Sources of error in bone mineral density estimates from quantitative CT," Eur J Radiol, tom 144, nr 110001, Nov 2021. https://doi.org/10.1016/j.ejrad.2021.110001.

[30] A. Pearce, R. Richards, S. Milz, E. Schneider, „Animal models for implant biomaterial research in bone: a review," Eur Cell Mater, tom 13, pp. 1-10, 2007. doi: https://doi.org/10.22203/ecm.v013a01.

[31] A. Inui, K. Itamoto, T. Takuma, et al., Age-Related Changes of Bone Mineral Density and Microarchitecture in Miniature Pigs, The Journal of veterinary medical science 66 (6), 599-609, 2004 doi: https://doi.org/10.1292/jvms.66.599

[32] J. Aerssens, S. Boonen, G. Lowet, J. Dequeker, „Interspecies differences in bone composition, density, and quality: potential implications for in vivo bone research," Endocrinology, tom 139, nr 2, pp. 663-670, 1998. doi: https://doi.org/10.1210/endo.139.2.5751.